

Topological quantum states of matter in iron-based superconductors: From concepts to material realization

Ning Hao^{1,*} and Jiangping Hu^{2,3,4,†}

¹Anhui Province Key Laboratory of Condensed Matter Physics at Extreme Conditions,
High Magnetic Field Laboratory of Chinese Academy of Sciences, Hefei 230031 China

²Beijing National Laboratory for Condensed Matter Physics,
and Institute of Physics, Chinese Academy of Sciences, Beijing 100190, China

³CAS Center of Excellence in Topological Quantum Computation and Kavli Institute of Theoretical Sciences,
University of Chinese Academy of Sciences, Beijing, 100190, China

⁴Collaborative Innovation Center of Quantum Matter, Beijing, 100871, China

(Dated: November 12, 2018)

We review recent progress in the explorations of topological quantum states of matter in iron-based superconductors. In particular, we focus on the nontrivial topology existing in the band structures and superconducting states of iron's 3d orbitals. The basic concepts, models, materials and experimental results are reviewed. The natural integration between topology and high-temperature superconductivity in iron-based superconductors provides great opportunities to study topological superconductivity and Majorana modes at high temperature.

Keywords: iron-based superconductor, topological insulator, topological superconductor, spin-orbit coupling

I. INTRODUCTION

In the past decade, topology becomes an essential ingredient to classify various types of materials, including insulators/semiconductors, semimetals and superconductors[1–3]. The physical consequence in a topological material is the existence of topologically protected surface states, which can be measured directly in transport, angle resolved photoemission spectrum(ARPES), scanning tunneling microscopy(STM) and other experiments[1–3]. In particular, in a topological superconductor, there are surface bound states, Majorana modes, which can be used to realize topological quantum computing because of their topological protection and non-Abelian braiding statistics[4].

While naturally-born topological superconductors are very rare, the realization of Majorana modes can be achieved in many artificial hybrid systems. Recently, a wealth of proposals for such experimental designs has been proposed, including the superconducting surface states of a topological insulator in proximity to conventional superconductors[5], quantum wires with strong spin-orbit coupling in proximity to conventional superconductors[6], semiconductor-superconductor heterostructures[7], and spin-chains embedded in conventional superconductors[8] etc. However, these hybrid systems, in general, have two shortcomings. First, it is always difficult to manage the interface between two different structures. Second, in all these proposals, as the proximity effect requires a long superconducting coherent length, high temperature superconductors, such as cuprates and iron-based super-

conductors, have never been candidates in those integration processes because of their extreme short coherent lengths and structural incompatibility. Thus, all devices require to be operated at very low temperature.

The above shortcomings can be overcome if we can find a high temperature superconductor which hosts nontrivial topological band structures. Specifically, to differentiate them from topological superconductors as well as the above hybrid superconducting systems, we refer this type of superconductors specifically as *connate* topological superconductors[9]. The connate topological superconductor can be viewed as an internal hybrid system which has conventional superconductivity in bulk but topological superconductivity on surface caused by the nontrivial topology on some part of band structures[9, 10]. Because of this intrinsic hybridization, the superconductor, in general, must be a multiple band electronic system. As iron-based high temperature superconductors are known to be multi-orbital electronic systems, they become promising candidates.

During the past several years, starting from theoretical understanding, the research of iron-based superconductors as connate topological superconductors has gradually been materialized. The first theoretical study of nontrivial band topology was carried out by us for the single layer FeSe/STO, in which a band inversion can take place at M points[11] to create nontrivial topology. Very quickly, it was found that the band inversion can easily take place at Γ point if the anion height from Fe layers are high enough. For FeSe, the height can be increased by substituting Se with Te[12, 13]. For ironpnictides, the As height is predicted to be high enough in the 111 series, LiFeAs to host nontrivial topology[14]. Besides these intrinsic topological properties from the Fe d-orbitals, nontrivial topology can also stem from bands outside Fe layers. For example, the As p-orbitals in the As layers of the 122 CaFeAs₂ are shown to be de-

*Electronic address: haon@hmfl.ac.cn

†Electronic address: jphu@iphy.ac.cn

scribed by a model similar to the Kane-Mele model in graphene[15]. Most recently, because of the improvement of sample quality and experimental resolutions, there have been increasing experimental evidence for topological properties in iron-based superconductors[16–18]. The theoretically predicted band inversions, together with the topologically protected surface states, have been directly observed. The Majorana-like modes are observed in several iron-chalcogenide materials[17, 18]. All these progresses have made iron-based superconductors to be a new research frontier for topological superconductivity.

In this paper, we give a brief review of both theoretical and experimental results regarding of the topological properties of iron-based superconductors. In section II, we discuss theoretical concepts and models for the topological band structure in iron-based superconductors and recent experimental evidence. In section III, we review topological superconductivity that can be emerged from the topological bands of iron-based superconductors and experimental evidence of Majorana-like modes in these materials. Finally, we will address open issues in this field.

II. TOPOLOGY IN IRON D-ORBITAL BANDS

A. Concepts and models

Since the discovery of iron-based superconductors in 2008, there has been remarkable progress in material growth and synthesis about the iron-based compounds. According to the element composition, the iron-based superconductors are classified into different categories denoted with “1111”, “122”, “111”, “11”, etc[19]. All categories possess the kernel substructure of X-Fe-X trilayer with X denoting As, P, S, Se, Te, as shown in Fig.1 (a). The X-Fe-X trilayer is the basic unit cell to give arise to magnetism and superconductivity, and play a similar role as Cu-O plane in cuprates. Following the principle from complexity to simplicity, the X-Fe-X trilayer skips the specificity among all the compounds in iron-based superconductors and brings the intrinsic physics to the surface. However, along the opposite logic, the diversity may include important subtle surprising differences. For iron-based superconductors, such kinds of accidental surprises can be intuitively demonstrated through evaluating the sensitivity of the electronic structures upon the tiny change of the structure of the X-Fe-X trilayer[20]. Fig.1 (c) gives such intuitive demonstration. The band structures sensitively depend on the fine tune of the distances between Fe-Fe and Fe-X. In particular, the bands switch orders near Γ point, a band gap opens near M point and the bands become strongly dispersive along $\Gamma - Z$ direction when the third dimension is considered. Indeed, the layered structures of the iron-based superconductors provide the possibilities to tune the distances between Fe-Fe and Fe-X. For example, the La-O layer in LaOFeAs and the Ba-As layer in BaFe₂As₂ naturally

cause different lattice constants for Fe-X layers[21, 22]. A variety of materials in the family of iron-based superconductors provide different fine-tuned X-Fe-X trilayers.

The band fine tuning would become nontrivial if there exist a topological phase transition. The discovery of topological insulators has established a standard paradigm about the topological quantum states of matter, which includes band inversion, bulk-boundary correspondence and relationship between symmetry and topological invariant etc[1, 2, 26–33]. For example, the first experimentally confirmed two-dimensional topological insulator, HgTe/CdTe quantum well, has a band inversion induced by the large spin-orbit coupling from Hg, depending on the thickness of the well, to give arise to a topological insulating state[27, 28]. The well-known three-dimensional topological insulators, Bi₂Se₃ and Bi₂Te₃, has a band inversion caused by a strong spin-orbit coupling that switch two p_z-type bands with opposite spatial-inversion-symmetry parities at the Γ point[33–35]. The picture of band inversion can be further simplified into the energy level shift in atomic limit through the adiabatic deformations[34]. Fig. 1 (d) gives the typical picture of energy level shift under the influence of several kinds of interactions in Bi₂Se₃[24].

Interestingly, a similar picture also exists in some specific iron-based superconductors with fine-tuned X-Fe-X layers. The typical picture of energy level shift of iron *d*-orbitals are shown in Fig. 1 (e) and (f) for Γ point in (e) and M point in (f), respectively. Note that the space group of Fe-X-Fe trilayer is P4/nmm, in which the glide-plane mirror symmetry operation $\{m_z|\frac{1}{2}\frac{1}{2}0\}$ and inversion symmetry operation $\{i|\frac{1}{2}\frac{1}{2}0\}$ are essential[11, 36–38]. First, the Bloch states can be classified according to the parities of $\{m_z|\frac{1}{2}\frac{1}{2}0\}$, i.e., $|d_{o/e,\alpha}\rangle$ or $|d_{o/e}, m_l, m_j\rangle$ with *o*, *e*, α , m_l , m_j denoting the odd or even parity of $\{m_z|\frac{1}{2}\frac{1}{2}0\}$, the α th *d* orbital, and two magnetic quantum numbers, respectively. Second, under the inversion symmetry operation $\{i|\frac{1}{2}\frac{1}{2}0\}$, the inversion parities of $|d_{o/e,\alpha}\rangle$ and $|d_{o/e}, m_l, m_j\rangle$ for $\alpha = xz/yz$, $m_l = \pm 1$ are opposite to the inversion parities of $|d_{o/e,\alpha}\rangle$ for $\alpha = xy$. Focus on the green rectangles in Fig. 1 (e) and (f), the spin-orbit coupling can switch the order of the energy levels with opposite inversion parities and induce a topological phase transition[11, 37, 38].

In early 2014, the authors of this paper noted that a tiny band gap around M point in the band structure of monolayer FeSe/SrTiO₃(FeSe/STO)[39] from measurement of the ARPES[40–45] and predicted the topological phase transition in this two-dimensional system [11]. It is the first proposal to discuss the topological quantum state of matter in iron-based superconductors. Corresponding to Fig. 1 (f), an effective $\mathbf{k}\cdot\mathbf{p}$ model can be constructed in the basis set of $\{|\psi_o\rangle\}, \{|\psi_e\rangle\}$ with $\{|\psi_o\rangle\} = \{|d_{o,xy,\uparrow}\rangle, |d_o, 1, \frac{3}{2}\rangle, |d_{o,xy,\downarrow}\rangle, |d_o, -1, -\frac{3}{2}\rangle\}$ and $\{|\psi_e\rangle\} = \{|d_{e,xy,\uparrow}\rangle, |d_e, -1, \frac{1}{2}\rangle, |d_{e,xy,\downarrow}\rangle, |d_e, 1, -\frac{1}{2}\rangle\}$

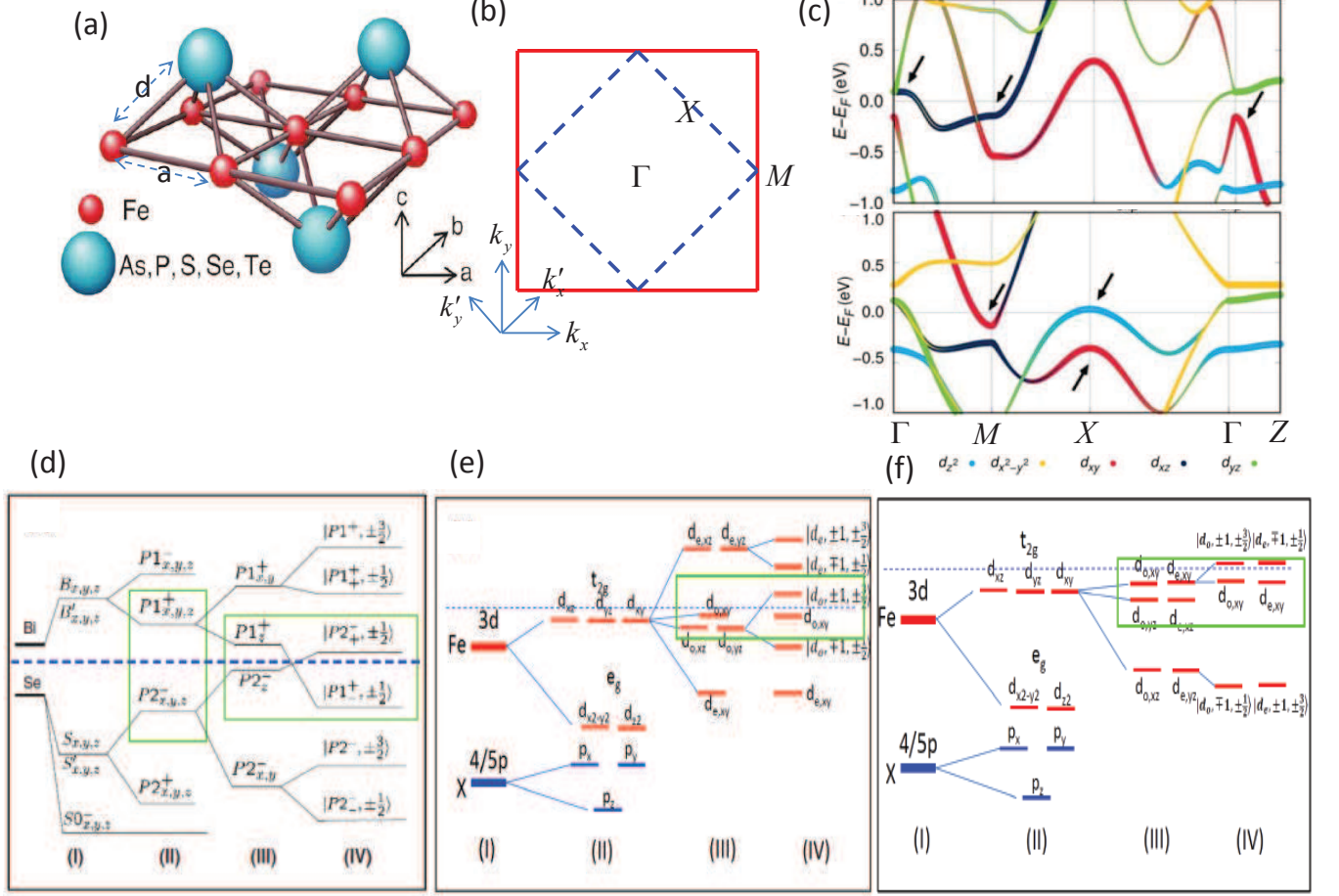


FIG. 1: (Color Online) (a) The structure of X-Fe-X trilayer. The distance between the nearest neighbor two ions/ion and X is label with a and d . (Adopted from [23]) (b) The Brillouin zone with high-symmetry point. The red solid/blue dashed lines label the Brillouin zone with one-iron/two-iron unit cell. In (c) the top/bottom panels correspond to parameters $(a, d)=(0.93, 0.98)/(1.09, 1)$ in unit of experimental values of FeSe[20]. (d) Schematic picture of the origin of the band structure of Bi₂Se₃. Starting from the atomic orbitals of Bi and Se, the following four steps are required to understand the band structure: (I) the hybridization of Bi orbitals and Se orbitals, (II) the formation of the bonding and antibonding states due to the inversion symmetry, (III) the crystal field splitting, and (IV) the influence of the spin-orbit coupling, from [24]. (e) and (f) the similar processes in iron-based superconductors at high-symmetry point Γ in (e) and point M in (f), from [25]. In both (e) and (f), (I) the hybridization of iron 3d orbitals and X 4p or 5p orbitals, (II) the crystal field splitting, (III) the formation of the bonding and antibonding states, which are classified with the parities of glide-plane symmetry, and (IV) the influence of the spin-orbit coupling or other effects.

$$H_M(k) = \begin{bmatrix} H_M^o(k) & H_c \\ H_c & H_M^e(k) \end{bmatrix}. \quad (1)$$

Here,

$$H_M^o(k) = \begin{bmatrix} H(k) & 0 \\ 0 & H^*(-k) \end{bmatrix}, \quad (2)$$

$H_M^e(k) = H_M^{o*}(-k)$, $H(k) = \varepsilon(k) + d_i(k)\sigma_i$ with $\varepsilon(k) = C - D(k_x^2 + k_y^2)$, $d_1(k) + id_2(k) = A(k_x + ik_y)$, and

$d_3(k) = M - B(k_x^2 + k_y^2)$ with $MB > 0$. In the absence of H_c term, the Hamiltonian in Eq.(1) reduces into two copies of Bernevig-Hughes-Zhang (BHZ) model[27], which is the standard model for quantum spin Hall effect. In each subspace with odd or even parity, a topological invariant $Z_2 = 1$ can be defined. Actually, H_c term is from the spin-flipped term $\lambda_{so}(L_x s_x + L_y s_y)$, which mixes the orbitals with odd and even parities of $\{m_z | \frac{1}{2} \frac{1}{2} 0\}$. As a consequence, the parity of $\{m_z | \frac{1}{2} \frac{1}{2} 0\}$ is no longer a good quantum number. The two subspaces couple with each other. The topological states is more like weak type.

can be called topological Dirac semimetal states when the chemical potential is moved to the cross point. This state can also be described by the effective model in Eq. (7). The target materials include Fe(Te,Se) and Li(Fe,Co)As[14, 46].

B. Materials and experiments

The three typical materials to realize the aforementioned topological quantum states of matter described by the three effective $\mathbf{k}\cdot\mathbf{p}$ Hamiltonian are monolayer FeSe/STO, monolayer FeTe_{1-x}Se_x/STO and FeTeSe single crystal. To experimentally identify these topological states, scanning tunneling microscopy/spectroscopy (STM/S) and ARPES are very powerful tools. STM/S is a real space surface measurement technique that measures the density of states as a function of position, and can be used to distinguish the edge states from bulk states[48, 49]. ARPES is a momentum space measurement technique that can directly read out the band structure, and can be used to evaluate the band evolution. The experimental results from STM/S and ARPES for these three materials are summarized in Fig. 2.

For monolayer FeSe/STO, the idea is based on comparing the gap (band gap and superconducting gap) from dI/dV of STS with the energy distribution curve (EDC) of ARPES in Fig. 2 (a) to determine the bulk gap. Then, the topological states possess the edge states, which cross the bulk band gap and are different from the trivial normal chemical edge states[47]. The contribution to the density of states from the topological edge states can be extracted by comparing the STS spectra between the bulk regime and the edge regime. Fig. 2 (c) and (d) are theoretical and experimental results, respectively. The key experimental observations are shown in Fig. 2 (c), from which, one can find that there exists some additional states from the edges after subtracting the contributions from the bulk background. However, only this feature is not enough to prove the nontrivial characteristics of the edge states. The trivial edge states can also have similar dI/dV behaviors. In Ref.[47], the checkerboard antiferromagnetic order is assumed to exist to open a trivial gap around M point in the monolayer FeSe/SrTO. In Ref.[11], the trivial band gap at M point is natural by taking into account the tension from SrTiO₃ substrate. Furthermore, the coexistence of antiferromagnetic order and superconducting order is doubtful in monolayer FeSe/STO, because the gap from the antiferromagnetic order is about 50meV, which should be easily to detect. For example, the gap should disappear above the antiferromagnetic transition temperature T_N . Thus, the nontrivial characteristics of the edge states should be further tested by other experimental method such as the spin-resolved STM or nonlocal transport[50].

In Fe(Te,Se) thin films, the topological phase transition appears when increasing the Te substitution of Se. Pictorial band evolution as change as Te substitution is a

promising evidence to testify the topological phase transition in Fe(Te,Se) thin film. Therefore, ARPES experiment is the primary choice. Fig. 2 (h) summarizes the band dispersions at Γ point for the samples with different x . The experiment results show that a down-shifting electron-like band move towards the hole-like and the band gap between them decreases rapidly when the Se content remains shrinks. Eventually the bands touch each other at a Se concentration of approximately 33%, which is further revealed in the plots of the constant energy contours and momentum distribution curves, as shown in Fig. 2 (e)-(g). The touch point corresponds to the critical point of band inversion. The ARPES experimental results give the indirect evidence for the topological band structure in monolayer FeTe_{1-x}Se_x/STO[9].

For the bulk FeTe_{1-x}Se_x single crystal, the emergence of electron band No. 4 in Fig. 2 (i) is the key ingredient to produce topological states when increasing the Te substitution of Se. The early ARPES experiment proved its existence through introducing the electron doping with *in situ* K evaporation[13]. The newly high energy and momentum resolution ARPES (HR-ARPES) (Energy resolution $\sim 70 \mu\text{eV}$) and the spin-resolved ARPES (SARPES) (Energy resolution $\sim 1.7 \text{ meV}$) provide powerful tools to directly observe the topological surface states and their spin polarization. Fig. 2 (j) and (k) clearly demonstrate the topological surface states with Dirac cone structure. Fig. 2 (n)-(q) identify the helical spin structure of the topological surface states. The combination of HR-ARPES and SARPES results directly proved the topological band structure in the bulk FeTe_{1-x}Se_x single crystal[16]. Recently, the similar topological band structure has also been identified in Li(Fe,Co)As[14], which not only confirms theoretical predictions but also proves the generic existence of tunable topological states in iron-based superconductors.

III. CONNATE TOPOLOGICAL SUPERCONDUCTIVITY

A. Material proposals

As we have mentioned in the introduction, a standard topological superconductor requires an odd-parity pairing, as shown in Fig. 3 (c). The famous representative materials including Sr₂RuO₄[51] and doped topological insulators Cu_xBi₂Se₃ and Sr_xBi₂Se₃[52–59] are proposed to be potential topological superconductors. However, the experimental situation is far from definitive, because the odd-parity pairing imposes restrictions to the pairing in spin-triplet channel, which is very rare in solid-state materials. Therefore, the recent research mainly focuses on some artificial structures which use the proximity effect from conventional superconductors on the surface/edge states of the three/two-dimensional topological insulator, on semiconductor film/nanowire with strong Rashba spin-orbit coupling, and on iron atom chain[5–

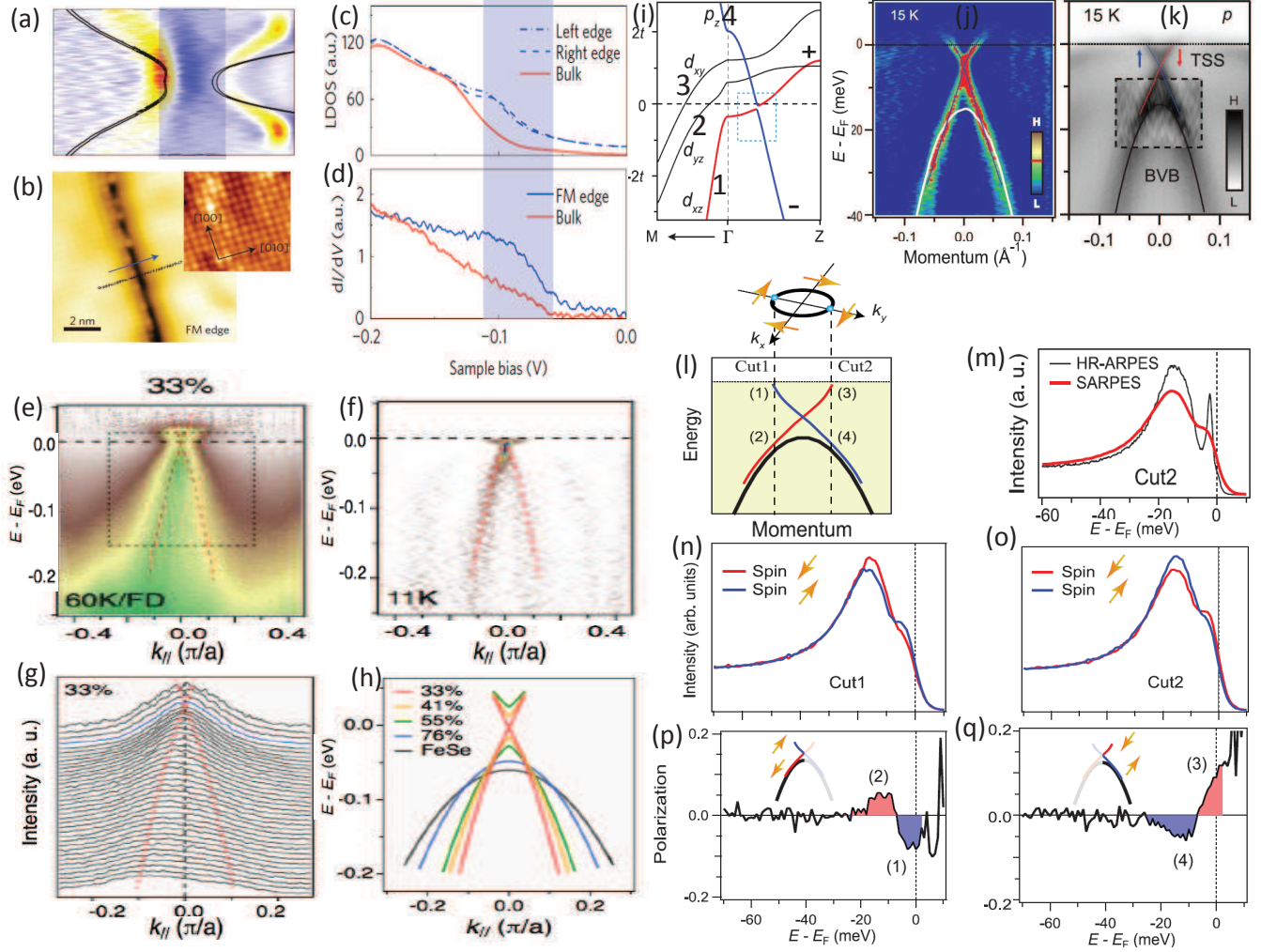


FIG. 2: (Color Online)(a)-(d) The ARPES and STM experimental results for monolayer FeSe/STO[47]. (e)-(f) The ARPES experimental results for monolayer Fe(Te_{1-x}Se_x)/STO[9]. (i)-(q) The ARPES experimental results for bulk Fe(Te,Se) single crystal[16]. (a) ARPES band structure around the M point. The black lines are theoretical band structures. (b) Experimental STM topography of the FM edge (0.1 nA, -300 mV) of FeSe/STO. The inset shows an atomic-resolution STM topography image at the bulk position of the FM edge (0.1 nA, 100 mV), showing the topmost Se atom arrangement (the crystal orientations are labelled). (c) Theoretical local density of states (LDOS) for edge and bulk states (d) Experimental STS spectra of edge and bulk states extracted from FM edges. The light blue band in (a), (c), (d) indicates the SOC gap. (e) The intensity plot divided by the Fermi-Dirac distribution function near Γ along the Γ - M direction for monolayer Fe(Te_{1-x}Se_x)/STO. (f) Curvature intensity plots along the same cut as in (e). The data were recorded at the temperature indicated in the panel. (g) MDC plot corresponding to the spectrum in the black square in (e). (h) Comparison of the band dispersions at Γ for the sample with different x . (i) First-principles calculations of band structure along Γ - M and Γ - Z . The dashed box shows the SOC gap of the inverted bands. (j) MDC curvature plot of the band data from ARPES, which enhances vertical bands (or the vertical part of one band) but suppresses horizontal bands (or the horizontal part of one band). The red dots trace the points where the intensity of the MDC curvature exceeds the red bar in the color-scale indicator, and the blue lines are guides to the eye indicating the band dispersion. (k) Summary of the overall band structure. The background image is amix of raw intensity and EDC curvature (the area in the dashed box). The bottom hole-like band is the bulk valence band, whereas the Dirac-cone-type band is the surface band. (l) Sketch of the spin-helical FS and the band structure along k_y , the sample ΓM direction. The EDCs at cuts 1 and 2 were measured with SARPES. The spin pattern comes from the bottom surface. (m) Comparison of the EDCs from SARPES and HR-ARPES measurements. The large broadening in the SARPES measurement could be partly responsible for the small spin polarization.(n) Spin-resolved EDCs at cut 1. (p) Spin polarization curve at cut 1. (o and q) Same as (n) and (p), but for EDCs at cut 2. The measured spin polarizations are consistent with the spin-helical texture illustrated in (l).

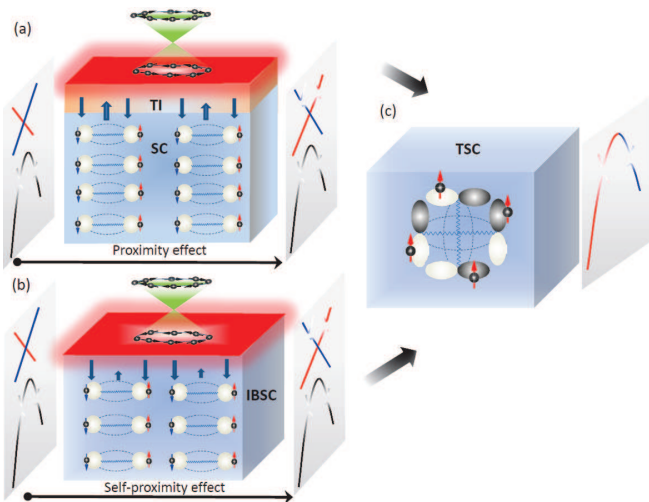


FIG. 3: (Color Online) Schematic illustrations of three kinds of strategies to realize topological superconducting states. (a) The hetero-structure involving conventional s-wave superconductor and topological insulator film. (b) The iron-based superconductors with topological surface states. (c) The unconventional superconductors with odd-parity pairing, i.e., the spin-polarized $p + ip$ pairing here.

7, 60–66], as shown in Fig. 3 (a). Effectively, the model described the structure in Fig. 3 (a) eventually reduce into the simpler model in Fig. 3 (c). The ultra-low superconducting transition temperature and the uncontrollability and uncertainty induced by the mismatch between different materials in the artificial structures take many undetermined problems and make these structures far beyond practicability[65, 66].

The superconductivity in iron-based superconductors is very robust against the fine tuning the band structures. Furthermore, the aforementioned topological phase transitions around Γ , M and Γ - Z line have no overall band gap because the iron-based superconductors are multi-orbital type and there exist other trivial bands across the Fermi energy besides the topological bands. When the temperature decreases below the superconducting transition temperature, the trivial bands across the Fermi energy open a superconducting gap due the formation of the cooper pairs. At the boundaries of the materials, the topological bands support the surface/edge states, which also cross the Fermi energy. In comparison with trivial or extrinsic proximity effect involving two different kinds of materials in Fig. 3 (a), the inducing superconductivity from trivial bulk bands to topological boundary bands happens in a single material, and can also be called intrinsic or self-proximity effect, as shown in Fig. 3 (b). When the Fermi energy is close to the surface Dirac point to guarantee the good approximation of the linear dispersion of the surface Dirac band, the superconducting single Dirac band can be reduced into a spinless $p_x + ip_y$ superconductor[5, 67], which is a topological superconductor, as shown in Fig. 3 (c). When the π -flux vortex

is formed in the magnetic field, the effective topological superconductor can support the zero-energy vortex-line end states, which are called Majorana modes.

Keeping the aforementioned picture in mind, one can find that all iron-based superconductors with topological band structures can support topological superconductors. For the monolayer FeSe/STO, the heavy hole-doped case can support the topological edge states while the electron-doped case can support extremely high-temperature superconductivity. Then, the boundary between the hole-doped and electron-doped regimes in a single monolayer sample can produce one-dimensional topological superconductor. For monolayer FeTe $_{1-x}$ Se $_x$ /STO, the superconductivity is robust in the whole doping regime[9]. The topological edge states emerge when $x < 0.33$, and the cooper pairs from the electron bands near M point can be scattered into the topological edge states from topological bands near Γ point. Then, the system spontaneously transform into the topological superconductor. For (Ca,Pr)FeAs $_2$ and Ca $_{1-x}$ La $_x$ FeAs $_2$, the distorted As chains in CaAs layers support topological edge states through the topological bands near B points, while the FeAs layers support superconductivity through the trivial bulk band near both Γ and M points. The self-proximity effect can induce the one-dimensional topological superconductivity in both (Ca,Pr)FeAs $_2$ and Ca $_{1-x}$ La $_x$ FeAs $_2$ [15, 68]. For bulk FeTe $_{1-x}$ Se $_x$ single crystal, the topological Dirac-cone type surface states emerge at $\bar{\Gamma}$ point in the (001) surface Brillouin zone in the topological doped regime. Then, the cooper pairs from the trivial bulk bands near Γ - Z line and the M - A line can be scattered into the topological Dirac-cone type surface states. These primary and secondary self-proximity effect can drive the bulk FeTe $_{1-x}$ Se $_x$ single crystal into the two-dimensional topological superconductor.

B. Experiments and open questions

For the monolayer FeSe/STO and FeTe $_{1-x}$ Se $_x$ /STO, the monolayer FeSe and FeTe $_{1-x}$ Se $_x$ grow on the substrate STO through the assistant of molecular beam epitaxy (MBE). Until now, both systems have the highest superconducting transition temperature among all iron-based superconductors, whereas they are unstable in the air. The shortcoming takes challenges to the devices fabrication and relevant transport measurement. On a contrary, the bulk FeTe $_{1-x}$ Se $_x$ single crystal is quite stable and has nice (001) cleavage surface. More importantly, the topological superconducting states are two-dimensional. The spontaneously generated vortex under external magnetic field could bound Majorana zero-energy mode if the superconducting state is topological. Then, some experimental methods like ARPES and STM/S can be used to verify the topological superconducting state and detect the Majorana zero-energy modes. Based on these upsides, most experimental pro-

gresses are mainly made in the bulk $\text{FeTe}_{1-x}\text{Se}_x$ single crystal and $(\text{Li}_{0.84}\text{Fe}_{0.16})\text{OHFeSe}$ single crystal[16–18, 69, 70]. Along time line, we review these experiments in the following.

The first unexpected experiment is about the impurity bound states in $\text{FeTe}_{0.57}\text{Se}_{0.43}$ single crystals[69]. $\text{FeTe}_{0.57}\text{Se}_{0.43}$ single crystals contain a large amount of excess iron that as single iron atoms randomly situate at the interstitial sites between two (Te, Se) atomic planes[71]. The STM/S spectrum observed a strong zero-energy bound state at the centre of the single interstitial Fe impurity. The experimental results are summarized in Fig. 4 (a)-(f). The zero-energy bound state has the following features. (1) The spatial pattern of the zero-energy bound state is almost circular, which is different from the cross-shape pattern of the Zn impurity in $\text{Bi}_2\text{Sr}_2\text{Ca}(\text{Cu},\text{Zn})_2\text{O}_{8+\delta}$ [72]. (2) The intensity of the zero-energy bound state exponentially decays with a characteristic length of $\xi = 3.5\text{\AA}$, which is almost one order of magnitude smaller than the typical coherent length of 25\AA in the iron-based superconductor[73, 74]. (3) The bound state is strictly at zero even the external magnetic field increases to 8T. (4) The zero-energy bound state peak remains at zero energy even when two interstitial Fe impurity atoms are located near each other ($\sim 15\text{\AA}$). It is a serious challenge to consistently explain these features of the zero-energy bound state induced by interstitial Fe impurity. The d-wave pairing symmetry scenario can result in a zero-energy bound state at unitary limit[75], but violates feature (1). The Kondo impurity resonance scenario can give an accidental zero-energy bound state[75], but violates feature (4). A fascinating scenario is that the mode is Majorana zero-energy mode[76, 77], which captures features (1)-(3). Recently, a theoretical work claimed that an interstitial Fe impurity could bound an quantum anomalous vortex without magnetic field, and the quantum anomalous vortex can bound a Majorana zero-energy mode when topological surface states of $\text{FeTe}_{0.57}\text{Se}_{0.43}$ become superconducting[78]. However, it is still hard to explain feature (4) by the Majorana zero-energy mode scenario. Until now, the origin of the zero-energy bound state trapped by interstitial Fe impurity is still underdetermined. Topological or other reasons need further experimental and theoretical explorations.

The second experimental breakthrough is about the vortex bound states on the surface of $\text{FeTe}_{0.55}\text{Se}_{0.45}$ single crystals[17, 70]. $\text{FeTe}_{0.55}\text{Se}_{0.45}$ belongs to type II superconductor. Once a small external magnetic field is applies along c-axis, magnetic vortex structures are formed due to the small lower critical field H_{c1} . The high-resolution STM/S can measure the bound states trapped by the vortex. Two experimental group claimed completely different results for the same material $\text{FeTe}_{0.55}\text{Se}_{0.45}$ single crystals. The former group claimed that they observed a sharp zero-bias peak inside a vortex core that does not split when moving away from the vortex center, which could be attributed to the nearly pure Majorana bound state[17]. The experimental results are summarized in

Fig. 4 (g)-(j). The vortex bound states exhibit the following features. (1) Statistically, there are about 20% success rate in observing the isolated pure Majorana bound state during more than 150 measurements. (2) Across a large range of magnetic fields the observed zero-bias peak does not split when moving away from a vortex center. (3) Most of the observed zero-bias peak vanish around 3K. (4) Robust zero-bias peaks can be observed over two orders of magnitude in tunneling barrier conductance, with the width barely changing. Feature (1) is argued to attribute to the disorder effect and/or inhomogeneous distribution of Te/Se. Feature (2) is attributed to the large Δ_{sc}/E_F ratio in this system. Feature (3) is attributed to that the Caroli-de-Gennes-Matricorn (CdGM) state[79] is protected by a mini-energy gap with with a temperature about $\Delta_{sc}^2/E_F \sim 3\text{K}$, and the thermal excitation around and beyond 3K can kill the CdGM state. Feature (4) indicated the line width of zero-bias peaks is almost completely limited by the combined broadening of energy resolution and STM thermal effect, suggesting that the intrinsic width of the Majorana bound state is much smaller in the weak tunnelling regime[80, 81]. The detailed experimental measurements eliminate some scenarios to cause a zero-bias peak in tunneling experiments, such as antilocalization, reflectionless tunneling, Kondo effect, Josephson supercurrent and packed CdGM states near zero energy[56, 82–88]. Features (2)-(4) can be well understood with the Majorana bound state scenario, it is probable that the observed zero-bias peaks correspond to Majorana bound state. However, the feature (1) is a serious problem, which is different from other proposals to realize Majorana bound states. In the present experiments, it seems no comprehensive evidences of the disorder effect and/or influence of inhomogeneous distribution of Te/Se are provided. Furthermore, if the observed zero-bias peaks are from Majorana bound states, the non-Abelian statistics can be demonstrated by move a vortex with a STM tip. This kind of experiment is the smoking gun for Majorana modes. Another experimental group claimed that they only observed the trivial CdGM bound state trapped by vortex in the same $\text{FeTe}_{0.55}\text{Se}_{0.45}$ single crystals. For statistics, the energies of bound state peaks close to the zero bias are collected from all measured nine vortices presented[70]. The experimental results are summarized in Fig. 4 (k)-(l). In principle, there should be a special vortex to bound the zero-bias peak according to the 20% success rate claimed in the former experiment. Unfortunately, two experiments for the same material from two groups give the inconsistent results[17, 70]. The argument about the difference being attributed to the different annealed process is not very convincing. It seems that the appearance of zero-bias peaks is selective. The behaviors challenge the topological origin, which is usually universal and robust.

The third subsequent experiment is about the vortex bound states on the FeSe cleavage plane of $(\text{Li}_{0.84}\text{Fe}_{0.16})\text{OHFeSe}$ single crystal[18]. In compared with $\text{FeTe}_{0.55}\text{Se}_{0.45}$, the superconducting FeSe layers

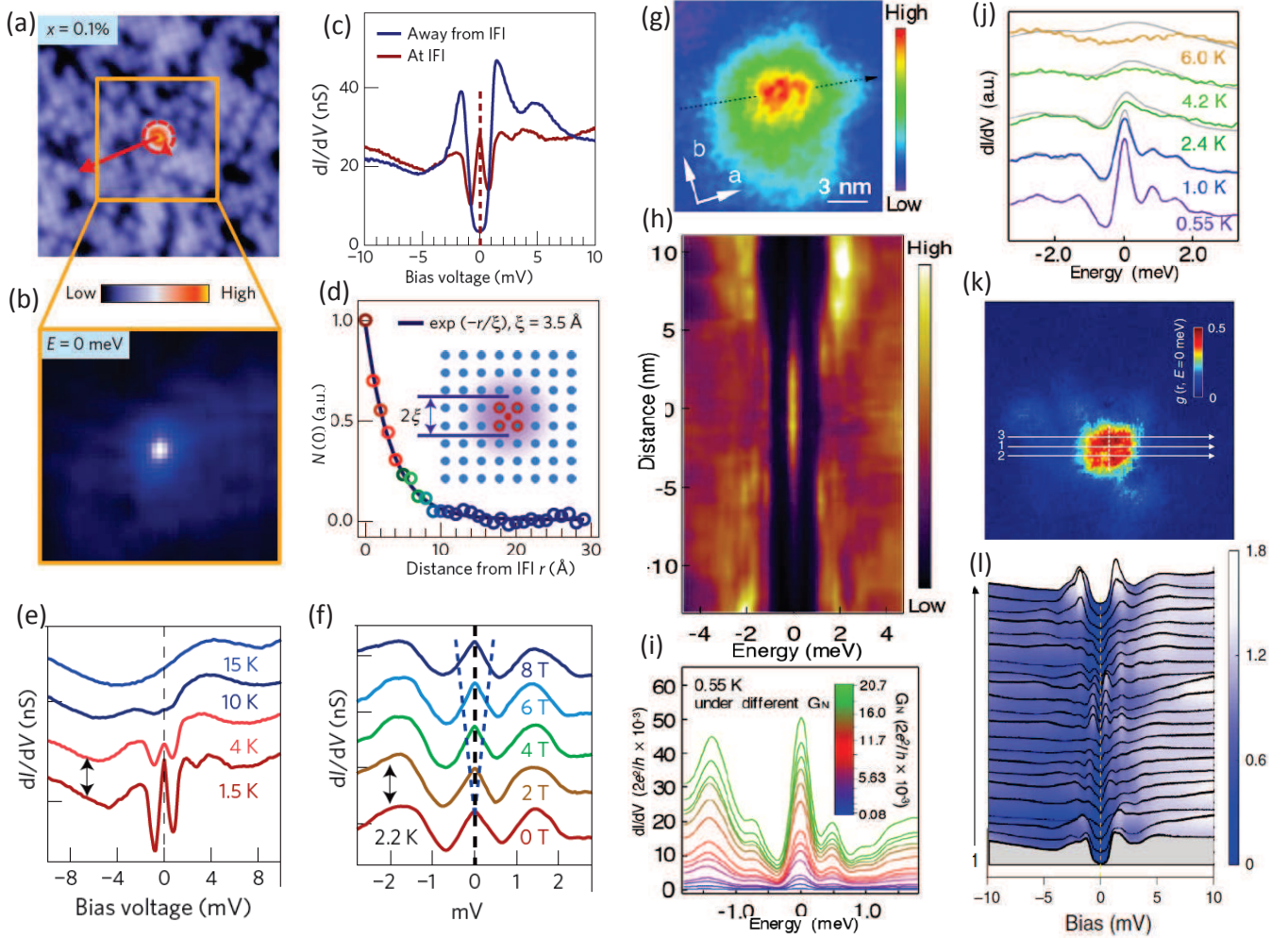


FIG. 4: (Color Online) (a)-(f) The STM/S experimental results for zero-bias states trapped by interstitial Fe impurity in $\text{FeTe}_{0.57}\text{Se}_{0.43}$ [69]. (g)-(l) The STM/S experimental results for bound states trapped by vortex in $\text{FeTe}_{0.55}\text{Se}_{0.45}$ [17, 70]. (a) Topographic image of an isolated single interstitial Fe impurity ($100 \times 100 \text{ \AA}$). (b) Zero-energy map for the area boxed in (a). (c) Spectra taken on top of and away from the interstitial Fe impurity. (d) Zero-energy peak value $N(0)$ versus distance r from single interstitial Fe impurity. The solid curve is an exponential fit with $\xi = 3.5 \text{ \AA}$. Inset is a schematic image for the spatial distribution of interstitial Fe impurity scattering. (e) The spectra taken at the same interstitial Fe impurity at different temperatures. (f) The spectra taken at the same interstitial Fe impurity under different magnetic fields. The blue V-shaped dashed line is a guide to the eye showing the expected Zeeman splitting ($g = 2$). (g) A zero-bias conductance map (area $15 \text{ nm} \times 15 \text{ nm}$) around vortex cores. (h) A line-cut intensity plot along the black dash line indicated in (g). (i) Evolution of zero-bias peaks with tunneling barrier measured at 0.55 K . $G_N = I_t/V_s$, which corresponds to the energy-averaged conductance of normal states, and represents the conductance of the tunneling barrier. I_t and V_s are the STS setpoint parameters. (j) Temperature evolution of zero bias peaks in a vortex core. The gray curves are numerically broadened 0.55 K data at each temperature. (k) Image of a single vortex in a $20 \text{ nm} \times 20 \text{ nm}$ region measured at 0.48 K and 4 T . (l) Tunneling spectra measured along the arrowed lines marked 1 in (k) with increment steps of 7.6 \AA . The dashed line shows the position of zero bias voltage. The discrete CdGM bound state peaks can be clearly observed near the vortex core center.

in $(\text{Li}_{0.84}\text{Fe}_{0.16})\text{OHFeSe}$ are stoichiometric. Therefore, there exist defect-free areas, which support the un-pinned or free vortex. The STM/S measurements show that (1) The free vortex cores bound zero-bias modes, which do not shift with varying underlying superconducting gap as the other peaks do. (2) the zero-bias modes survive to high magnetic field due to the short co-

herence length. (3) The zero-bias mode coexists with other low-lying CdGM states but separates from each other. These features are similar to those of the zero-bias modes observed in $\text{FeTe}_{0.55}\text{Se}_{0.45}$. Therefore, the zero-bias modes can be also attributed to Majorana zero-energy modes, and can be argued to have topological origin in $(\text{Li}_{0.84}\text{Fe}_{0.16})\text{OHFeSe}$. However, the topological

origin in $(\text{Li}_{0.84}\text{Fe}_{0.16})\text{OHFeSe}$ is underdetermined, unlike $\text{FeTe}_{0.55}\text{Se}_{0.45}$ with solid experimental evidences for the topological band structure. Recall the discussions about the band inversion along Γ - Z line in $\text{FeTe}_{0.55}\text{Se}_{0.45}$ in Section II A, the strong dispersion of band 4 in Fig. 2 (j) benefits from the quite small layer distance and large size of Te atoms. The band 4 in pure FeSe is flat[13]. It is very strange that the band 4 in $(\text{Li}_{0.84}\text{Fe}_{0.16})\text{OHFeSe}$ has strong dispersion. Furthermore, the band gap open is due to the strong spin-orbit coupling from Te atom not Se atom. Another critical condition to obtain the topological surface states is that the chemical potential must properly lie in the quite small band gap. However, the chemical potential in $(\text{Li}_{0.84}\text{Fe}_{0.16})\text{OHFeSe}$ is far from the band gap. In this situation, the top and bottom surfaces start to communicate with each other and break the zero-bias mode. At last, it lacks the smoking gun ARPES experiment to prove the helical structure of the claimed observed topological surface states in $(\text{Li}_{0.84}\text{Fe}_{0.16})\text{OHFeSe}$. In summary, the experimental observations of the zero-bias modes in $(\text{Li}_{0.84}\text{Fe}_{0.16})\text{OHFeSe}$ is more clear, but the topological origin needs to be understood.

IV. SUMMARY AND PERSPECTIVES

The discovery of topological insulators has established a standard paradigm to guide the communities to pursue the topological states of matter in quantum materials. Such pursuits cause intersections between the topology and iron-based superconductors. As emphasized in this review, important principles for the theoretical understandings of the energy-band topology in new materials include applying general concepts with the help of symmetry analysis and constructing the effective models. For the iron-based superconductors, the multi-orbital band structures and the diversity of materials provide opportunities to realize the effective theoretical models. These topological materials include monolayer FeSe/STO , monolayer $\text{Fe}_{1-x}\text{Se}_x/\text{STO}$, $\text{FeTe}_{1-x}\text{Se}_x$, and $\text{LiFe}_{1-x}\text{Co}_x\text{As}$ etc.

In the superconducting states, it is naturally expected to obtain the topological superconducting states with the help of self-proximity effect. However, different from the energy-band topology, the expected topological superconducting states exhibit many unexpected experimental phenomena, including the surprising robust zero-energy mode trapped by Fe impurity in $\text{FeTe}_{0.57}\text{Se}_{0.43}$, the selective appearance of zero-bias mode trapped by vortex in $\text{FeTe}_{0.57}\text{Se}_{0.43}$, and the coexistence of zero-bias mode and CdGM states trapped by free vortex in $(\text{Li}_{0.84}\text{Fe}_{0.16})\text{OHFeSe}$. Even if all these phenomena are attributed to Majorana zero-energy modes, there are deep inconsistencies within different experiments as well

as between experiments and theories. In this respect, clarifying the creation mechanism of these so-called Majorana zero-energy modes are worth pursuing. For such efforts, the availability of the high-quality single crystal, whose chemical potential can be artificially fine tuned, would be crucial. Once the physics of the so-called Majorana zero-energy modes are clarified, finding ways to manipulate the non-Abelian statistics of the Majorana zero-energy modes is a significant challenge for future applications in quantum computing.

Iron-based superconductor owns a rich phase diagram. Beside the normal and superconducting phases, there include nematic phase, orbital ordering phase and various antiferromagnetic phases. Searching the topology embedded in these ordered phases would be interesting. For the theoretical aspect, there have been some studies[89, 90], but the experimental exploration is blank. In future, a stronger collaboration between theory and experiment is required to explore topological quantum states in new materials of iron-based superconductors.

Finally, it can not be entirely ruled out that the superconducting states of iron-based superconductors themselves could be highly unconventional. In the ten years of the research of iron-based superconductors, there still are many unsolved puzzles[91, 92] observed by a variety of different experimental methods, such as transport, Raman spectrum, neutron scattering, nuclear magnetic resonance, electron spin resonance, STM/S, and ARPES etc. For example, the interplay between spin, orbital, lattice and charge degrees of freedom is not fully understood, not only is there no smoking gun proof for the s_{\pm} pairing yet but also it is clear that the s_{\pm} pairing symmetry cannot be valid for many iron-chalcogenide systems, whether there is a sign change in the superconducting states of iron-chalcogenide systems without hole pockets or not are highly debated, and the origin of the enhancement of the transition temperature found in single layer FeSe remains to be understood. The topological exploration in iron-based superconductors may help us to discover surprising characters and mechanism hidden behind superconducting pairing, and leads to answers to these unsolved puzzles.

Acknowledgments

N. Hao thanks the KITS, UCAS for the hospitality during his visit. This work was supported by the National Key R&D Program of China (No.2015CB921300, No.2017YFA0303100, 2017YFA0303201), National Natural Science Foundation of China (No. 11674331, No. 11334012), the ‘100 Talents Project’ of Chinese Academy of Sciences, and the Strategic Priority Research Program of CAS (No.XDB07000000).

[1] Hasan MZ and Kane CL. Colloquium: topological insulators. *Rev Mod Phys* 2010; **82**:3045.

[2] Qi XL and Zhang SC. Topological insulators and super-

- conductors. *Rev Mod Phys* 2011; **83**:1057.
- [3] Armitage NP, Mele EJ and Vishwanath A. Weyl and Dirac semimetals in three-dimensional solids. *Rev Mod Phys* 2018; **90**:015001.
 - [4] Nayak C, Simon SH and Stern A *et al.* Non-abelian anyons and topological quantum computation. *Rev Mod Phys* 2008; **80**:1083.
 - [5] Fu L and Kane CL. Superconducting proximity effect and majorana fermions at the surface of a topological insulator. *Phys Rev Lett* 2008; **100**:096407.
 - [6] Lutchyn RM, Sau JD and Sarma SD. Majorana fermions and a topological phase transition in semiconductor-superconductor heterostructures. *Phys Rev Lett* 2010; **105**:077001.
 - [7] Sau JD, Lutchyn, RM and Tewari S *et al.* Generic new platform for topological quantum computation using semiconductor heterostructures. *Phys Rev Lett* 2010; **104**:040502.
 - [8] Nadj-Perge S, Drozdov IK and Li J *et al.* Observation of majorana fermions in ferromagnetic atomic chains on a superconductor. *Science* 2014, 10.1126/science.1259327.
 - [9] Shi X, Han ZQ, Richard P *et al.* FeTe_{1-x}Se_x monolayer films: towards the realization of high-temperature nate topological superconductivity. *Science bulletin* 2017; **62**:503–507.
 - [10] Xu G, Lian B and Tang P *et al.* Topological superconductivity on the surface of Fe-based superconductors. *Phys Rev Lett* 2016; **117**:047001.
 - [11] Hao N and Hu J. Topological phases in the single-layer FeSe. *Phys Rev X* 2014; **4**:031053.
 - [12] Wu X, Qin S and Liang Y *et al.* Topological characters in Fe(Te_{1-x}Se_x) thin films. *Phys Rev B* 2016; **93**:115129.
 - [13] Wang Z, Zhang P and Xu G *et al.* Topological nature of the FeSe_{0.5}Te_{0.5} superconductor. *Phys Rev B* 2015; **92**:115119.
 - [14] Zhang P, Wu X and Yaji K *et al.* Direct observation of multiple topological phases in the iron-based superconductor Li(Fe,Co)As. *Nature Physics (online), arXiv:1803.00846* 2018.
 - [15] Wu X, Qin S and Liang Y *et al.* CaFeAs₂: A staggered intercalation of quantum spin Hall and high-temperature superconductivity. *Phys Rev B* 2015; **91**:081111.
 - [16] Zhang P, Yaji K and Hashimoto T *et al.* Observation of topological superconductivity on the surface of an iron-based superconductor. *Science* 2018; **360**:182–186.
 - [17] Wang D, Kong L and Fan P *et al.* Evidence for majorana bound states in an iron-based superconductor. *Science* 2018; **362**:333–335.
 - [18] Liu Q, Chen C and Zhang T *et al.* Robust and clean majorana zero mode in the vortex core of high-temperature superconductor (Li_{0.84}Fe_{0.16})OHFeSe. *arXiv:1807.01278 [cond-mat.supr-con]*, 2018.
 - [19] Paglione J and Greene RL. High-temperature superconductivity in iron-based materials. *Nat phys* 2010; **6**:645.
 - [20] Guterding D, Jeschke HO, and Valentí R. Basic electronic properties of iron selenide under variation of structural parameters. *Phys Rev B* 2017; **96**:125107.
 - [21] Singh DJ and Du MH. Density functional study of LaFeAsO_{1-x}F_x: A low carrier density superconductor near itinerant magnetism. *Phys Rev Lett* 2008; **100**:237003.
 - [22] Singh DJ. Electronic structure and doping in BaFe₂As₂ and lifas: Density functional calculations. *Phys Rev B* 2008; **78**:094511.
 - [23] Podolsky D. Untangling the orbitals in iron-based superconductors. *Physics* 2012; **5**:61.
 - [24] Liu C, Qi X and Zhang H *et al.* Model Hamiltonian for topological insulators. *Phys Rev B* 2010; **82**:045122.
 - [25] Hao N and J. Hu. Research progress of topological quantum states in iron-based superconductor. *Acta Phys Sin* 2018; **67**:207101.
 - [26] Kane CL and Mele EJ. Z₂ topological order and the quantum spin Hall effect. *Phys Rev Lett* 2005; **95**:146802.
 - [27] Bernevig BA, Hughes TL and Zhang S. Quantum spin Hall effect and topological phase transition in HgTe quantum wells. *Science* 2006; **314**:1757–1761.
 - [28] König M, Wiedmann S and Brüne C *et al.* Quantum spin Hall insulator state in HgTe quantum wells. *Science* 2007; **318**:766–770.
 - [29] Moore JE and Balents L. Topological invariants of time-reversal-invariant band structures. *Phys Rev B* 2007; **75**:121306.
 - [30] Fu L, Kane CL, and Mele EJ. Topological insulators in three dimensions. *Phys Rev Lett* 2007; **98**:106803.
 - [31] Roy R. Topological phases and the quantum spin Hall effect in three dimensions. *Phys Rev B* 2009; **79**:195322.
 - [32] Fu L and Kane CL. Topological insulators with inversion symmetry. *Phys Rev B* 2007; **76**:045302.
 - [33] Chen Y, Analytis JG, Chu J *et al.* Experimental realization of a three-dimensional topological insulator, Bi₂Te₃. *Science* 2009; **325**:178–181.
 - [34] Zhang H, Liu C and Qi X *et al.* Topological insulators in Bi₂Se₃, Bi₂Te₃ and Sb₂Te₃ with a single Dirac cone on the surface. *Nat phys* 2009; **5**:438.
 - [35] Xia Y, Qian D and Hsieh D *et al.* Observation of a large-gap topological-insulator class with a single Dirac cone on the surface. *Nat phys* 2009; **5**:398.
 - [36] Cvetkovic V and Vafeek O. Space group symmetry, spin-orbit coupling, and the low-energy effective Hamiltonian for iron-based superconductors. *Phys Rev B* 2013 **88**:134510.
 - [37] Hao N and Hu J. Odd parity pairing and nodeless antiphase S_± in iron-based superconductors. *Phys Rev B* 2014; **89**:045144.
 - [38] Hao N and Shen S. Topological superconducting states in monolayer FeSe/SrTiO₃. *Phys Rev B* 2015; **92**:165104.
 - [39] Wang Q, Li Z and Zhang W *et al.* Interface-induced high-temperature superconductivity in single unit-cell FeSe films on SrTiO₃. *Chin Phys Lett* 2012; **29**:037402, .
 - [40] He S, He J and Zhang W *et al.* Phase diagram and electronic indication of high-temperature superconductivity at 65 k in single-layer FeSe films. *Nat Mat* 2013; **12**:605.
 - [41] Tan S, Zhang Y and Xia M *et al.* Interface-induced superconductivity and strain-dependent spin density waves in FeSe/SrTiO₃ thin films. *Nat Mat* 2013; **12**:634.
 - [42] Liu D, Zhang W and Mou D *et al.* Electronic origin of high-temperature superconductivity in single-layer FeSe superconductor. *Nat Commun* 2012; **3**:931.
 - [43] Lee JJ, Schmitt FT and Moore RG *et al.* Interfacial mode coupling as the origin of the enhancement of T_c in FeSe films on SrTiO₃. *Nature* 2014; **515**:245.
 - [44] Miyata Y, Nakayama K and Sugawara K *et al.* High-temperature superconductivity in potassium-coated multilayer FeSe thin films. *Nat Mat* 2015 **14**:775.
 - [45] Peng R, Xu HC and Tan SY *et al.* Tuning the band structure and superconductivity in single-layer FeSe by interface engineering. *Nat Commun* 2014; **5**:5044.
 - [46] Zhang P, Wang Z and Ishida Y *et al.* Topological

- Dirac semimetal phase in the iron-based superconductor Fe(Te,Se). *arXiv:1803.00845 [cond-mat.supr-con]*, 2018.
- [47] ZF Wang, Zhang H and Liu D *et al.* Topological edge states in a high-temperature superconductor FeSe/SrTiO₃ (001) film. *Nat. Mater.* 2016; **15**:968.
- [48] Yang F, Miao L and Wang ZF *et al.* Spatial and energy distribution of topological edge states in single Bi(111) bilayer. *Phys Rev Lett*, 109(1):016801, 2012.
- [49] Drozdov IK, Alexandradinata A and Jeon S *et al.* One-dimensional topological edge states of bismuth bilayers. *Nat Phys*, 10:664, 2014.
- [50] Roth A, Brüne C and Buhmann H *et al.* Nonlocal transport in the quantum spin Hall state. *Science* 2009; **325**:294–297.
- [51] Mackenzie AP and Maeno Y. The superconductivity of Sr₂RuO₄ and the physics of spin-triplet pairing. *Rev Mod Phys*, 2003; **75**:657–712.
- [52] Fu L and Berg E. Odd-parity topological superconductors: theory and application to Cu_xBi₂Se₃. *Phys Rev Lett* 2010; **105**:097001.
- [53] Hor YS, Williams AJ and Checkelsky JG *et al.* Superconductivity in Cu_xBi₂Se₃ and its implications for pairing in the undoped topological insulator. *Phys Rev Lett* 2010; **104**:057001.
- [54] Kriener M, Segawa K and Ren Z *et al.* Bulk superconducting phase with a full energy gap in the doped topological insulator Cu_xBi₂Se₃. *Phys Rev Lett* 2011; **106**:127004.
- [55] Sasaki S, Kriener M and Segawa K *et al.* Topological superconductivity in Cu_xBi₂Se₃. *Phys Rev Lett* 2011; **107**:217001.
- [56] Levy N, Zhang T and Ha J *et al.* Experimental evidence for *s*-wave pairing symmetry in superconducting Cu_xBi₂Se₃ single crystals using a scanning tunneling microscope. *Phys Rev Lett* 2013; **110**:117001.
- [57] Mizushima T, Yamakage A and Sato M *et al.* Dirac-fermion-induced parity mixing in superconducting topological insulators. *Phys Rev B* 2014; **90**:184516.
- [58] Lahoud E, Maniv E and Petrushevsky MS *et al.* Evolution of the fermi surface of a doped topological insulator with carrier concentration. *Phys Rev B* 2013; **88**:195107.
- [59] Liu Z, Yao X and Shao J *et al.* Superconductivity with topological surface state in Sr_xBi₂Se₃. *J Am Chem Soc* 2015; **137**:10512–10515.
- [60] Alicea J. Majorana fermions in a tunable semiconductor device. *Phys Rev B* 2010; **81**:125318.
- [61] Mourik V, Zuo K and Frolov SM *et al.* Signatures of majorana fermions in hybrid superconductor-semiconductor nanowire devices. *Science* 2012; **336**:1003–1007.
- [62] Nadj-Perge S, Drozdov IK and Li J *et al.*, Observation of majorana fermions in ferromagnetic atomic chains on a superconductor. *Science* 2014 **346**:602–607.
- [63] Albrecht SM, Higginbotham AP and Madsen M *et al.* Exponential protection of zero modes in Majorana islands. *Nature* 2016; **531**:206.
- [64] Xu S, Alidoust N and Belopolski I *et al.*, Momentum-space imaging of cooper pairing in a half-Dirac-gas topological superconductor. *Nat Phys* 2014; **10**:943.
- [65] Xu J, Wang M and Liu Z *et al.* Experimental detection of a majorana mode in the core of a magnetic vortex inside a topological insulator-superconductor Bi₂Te₃/NbSe₂ heterostructure. *Phys Rev Lett* 2015; **114**:017001.
- [66] Sun H, Zhang K and Hu L *et al.* Majorana zero mode detected with spin selective Andreev reflection in the vortex of a topological superconductor. *Phys Rev Lett* 2016; **116**:257003.
- [67] Xu G, Lian B and Tang P *et al.* Topological superconductivity on the surface of Fe-based superconductors. *Phys Rev Lett* 2016; **117**:047001.
- [68] Wu X, Le C and Liang Y *et al.* Effect of As-chain layers in CaFeAs₂. *Phys Rev B* 2014; **89**:205102.
- [69] Yin JX, Wu Z and Wang JH *et al.* Observation of a robust zero-energy bound state in iron-based superconductor Fe(Te,Se). *Nat Phys*, 11(7):543, 2015.
- [70] Chen M, Chen X and Yang H *et al.* Discrete energy levels of Caroli-de Gennes-Matricon states in quantum limit in FeTe_{0.55}Se_{0.45}. *Nat Commun* 2018; **9**:970.
- [71] Taen T, Tsuchiya Y and Nakajima Y *et al.* Superconductivity at $T_c \sim 14$ K in single-crystalline FeTe_{0.61}Se_{0.39}. *Phys Rev B* 2009; **80**:092502.
- [72] Pan SH, Hudson EW and Lang KM *et al.* Imaging the effects of individual Zinc impurity atoms on superconductivity in Bi₂Sr₂CaCu₂O_{8+ δ} . *Nature* 2000; **403**:746.
- [73] Yin Y, Zech M and Williams TL Scanning tunneling spectroscopy and vortex imaging in the iron pnictide superconductor BaFe_{1.8}Co_{0.2}As₂. *Phys Rev Lett* 2009; **102**:097002.
- [74] Shan L, Wang Y and Shen B *et al.* Observation of ordered vortices with andreev bound states in Ba_{0.6}K_{0.4}Fe₂As₂. *Nat Phys* 2011; **7**:325.
- [75] Balatsky AV, Vekhter I and Zhu J. Impurity-induced states in conventional and unconventional superconductors. *Rev Mod Phys* 2006; **78**:373.
- [76] Read N and Green D. Paired states of fermions in two dimensions with breaking of parity and time-reversal symmetries and the fractional quantum Hall effect. *Phys Rev B* 2000; **61**:10267–10297.
- [77] Kitaev AY. Unpaired Majorana fermions in quantum wires. *Phys Usp* 2001; **44**:131.
- [78] Jiang K, Dai X and Wang Z. Quantum anomalous vortex and majorana zero mode in Fe (Te, Se) superconductors. *arXiv preprint arXiv:1808.07072*, 2018.
- [79] Caroli C, Gennes PGD and Matricon J. Bound fermion states on a vortex line in a type II superconductor. *Phys Lett*, 9:307–309, 1964.
- [80] Setiawan F, Liu C and Sau JD *et al.* Electron temperature and tunnel coupling dependence of zero-bias and almost-zero-bias conductance peaks in Majorana nanowires. *Phys Rev B* 2017; **96**:184520.
- [81] Colbert JR and Lee PA. Proposal to measure the quasi-particle poisoning time of Majorana bound states. *Phys Rev B* 2014; **89**:140505.
- [82] Pikulin DI, Dahlhaus JP and Wimmer M *et al.* A zero-voltage conductance peak from weak antilocalization in a Majorana nanowire. *New J Phys* 2012; **14**:125011.
- [83] Bagrets D and Altland A. Class *D* spectral peak in Majorana quantum wires. *Phys Rev Lett* 2012; **109**:227005.
- [84] Wees BJV, Vries PD and Magnée P *et al.* Excess conductance of superconductor-semiconductor interfaces due to phase conjugation between electrons and holes. *Phys Rev Lett* 1992; **69**:510–513.
- [85] Lee EJH, Jiang X and Aguado R *et al.* Zero-bias anomaly in a nanowire quantum dot coupled to superconductors. *Phys Rev Lett* 2012; **109**:186802.
- [86] Churchill HOH, Fatemi V and Grove-Rasmussen K *et al.* Superconductor-nanowire devices from tunneling to the multichannel regime: Zero-bias oscillations and magnetoconductance crossover. *Phys Rev B* 2013; **87**:241401.

- [87] Hess HF, Robinson RB, and Waszczak JV. Vortex-core structure observed with a scanning tunneling microscope. *Phys Rev Lett* 1990; **64**:2711–2714.
- [88] Gygi F and Schluter M. Electronic tunneling into an isolated vortex in a clean type-II superconductor. *Phys Rev B* 1990; **41**:822–825.
- [89] Wu X, Liang Y and Fan H *et al.* Nematic orders and nematicity-driven topological phase transition in FeSe. *arXiv:1603.02055 [cond-mat.supr-con]*, 2016.
- [90] Hao N, Zheng F and Zhang P *et al.* Topological crystalline antiferromagnetic state in tetragonal FeS. *Phys Rev B* 2017; **96**:165102.
- [91] Hirschfeld PJ, Korshunov MM and Mazin II. Gap symmetry and structure of Fe-based superconductors. *Rep Prog Phys* 2011; **74**:124508.
- [92] Chubukov AV and Hirschfeld PJ. Fe-based superconductors: seven years later. *arXiv preprint arXiv:1412.7104*, 2014.